Unveiling the Critical Intermediate Stages During Chemical Vapor Deposition of Two-Dimensional Rhenium Diselenide

Xin Chen[1+], Lok-Wing Wong[2+], Lingli Huang[1], Fangyuan Zheng[2], Rui Huang[3], Shu Ping Lau[2], Chun-Sing Lee[1], Jiong Zhao[2], Qingming Deng[3]*, Thuc Hue Ly[1]**

1 Department of Chemistry and Center of Super-Diamond & Advanced Films (COSDAF), City University of Hong Kong, Kowloon, Hong Kong 999077, China & City University of Hong Kong Shenzhen Research Institute, Shenzhen 518057, China.

2 Department of Applied Physics, The Hong Kong Polytechnic University, Kowloon, Hong Kong 999077, China & Polytechnic University of Hong Kong Shenzhen Research Institute, Shenzhen 518057, China.

3 Physics department and Jiangsu Key Laboratory for Chemistry of Low-Dimensional Materials, Huaiyin Normal University, Huaian 223300, China.

[+]Xin Chen and Lok-Wing Wong contributed equally in this work.

KEYWORDS

2D $ReSe_2$, cluster, nucleation, CVD, STEM

ABSTRACT

Two-dimensional (2D) transition metal dichalcogenides (TMDs) are promising materials for numerous emergent applications. Here we apply atomic-resolution scanning transmission electron microscopy (TEM) to resolve the intermediate stages during chemical vapor deposition (CVD) synthesis of 2D rhenium diselenide ($ReSe_2$). Contradicted to the conventional growth models proposed previously, stable intermediate species, *viz.* molecular metal chalcogenide clusters, are experimentally unveiled. These molecular clusters prevailed in chemical vapor deposition chamber can significantly alter the growth kinetics, the mass transport and surface anchoring sites. The new layer nucleation and the yielded flake morphology are both substantially influenced. Our work resolved the critical question on whether the nucleation occurs in atmosphere or on solid surface. Besides, additional experiments show that the hydrogen environment in CVD chamber can mitigate the aggregation problem of clusters, which is decisive for obtaining uniform 2D full films. Combined with density functional theory (DFT) calculations, the key reaction steps during growth are identified. Here, we show clear pictures on the debated growth mechanisms of 2D TMDs, expected to facilitate further optimization of CVD growth conditions to achieve stable mass production.

INTRODUCTION

Two-dimensional (2D) transition metal dichalcogenides (TMDs) hold the promise of new generation semiconductor device applications[1]. Due to the superior growth speed and relative low cost, chemical vapor deposition (CVD) is the most common synthesis method in semiconductor industry at present[2-4]. However, the greatest challenge in CVD growth of 2D TMDs, inaccessible to the accurate thickness control and perfect layer-by-layer growth, is retarding further

technological advances[5]. Although the thickness of 2D TMD can be controlled in CVD synthesis[6], and a number of precursors, including the metal oxides and chalcogenides for atmospheric pressure/low pressure CVD (APCVD/LPCVD)[7], the metalorganics for metal-organic CVD (MOCVD)[8], space-confined method of TMD under graphene on Au foils[9], solvent evaporation technique[10], as well as the different temperatures/pressures/substrates have been deployed by the CVD of 2D TMDs in previous works[11], however the control on morphology of 2D TMDs remain unresolved. The reaction sites, mass transportation pathways and intermediate species involved in growth are still under hot debate[12]. Undoubtedly, the clarification of kinetic reaction mechanisms of CVD growth of 2D TMDs will greatly benefit the synthesis, in terms of product quality and reproducibility, and will further influence widely on the relevant application fields[13].

Although the precursors of CVD of TMDs, and the structures of 2D TMDs are well known[14], the reaction kinetics in vapor or on solid surfaces[15] in CVD process are not well understood yet. Contradictory growth mechanisms have been proposed previously, mostly through simulations, such as reactions on oxide surfaces[16], intermediate MO_xC_y (M=transition metal, O=oxygen, C=chalcogenide) clusters[17], MC_2 clusters (M=transition metal, C=chalcogenide) [18,19], etc. The above reaction paths could impose different energy barriers for nucleation and growth, which may lead to inhomogeneities, defects and other non-equilibrium structures. To date, it remains difficult to yield the strict Frank-van der Merwe (FM) layer-by-layer growth of 2D TMDs by CVD[20], similarly for other atomically 2D films[21,22]. In case of 2D TMDs, it has been noted the anchoring of the precursors from vapor is crucial for the TMD growth[23,24]. The subsequent reactions and growth kinetics involve uncertain intermediate stages[12]. The speculated or simulated growth mechanisms need experimental verifications[25,26]. Owing to the ultrathin thickness of 2D layers and restrictions on CVD facility, normally it is hard to experimentally probe the reactants or species in

the ongoing CVD chambers. However, the intermediate stages during growth are possible to be "freezed" and studied *ex situ*.

In this work, we employ atomic-scale scanning transmission electron microscopy (TEM) to capture the intermediate clusters and cluster complexes during CVD growth of 2D rhenium diselenide ($ReSe_2$). These molecular clusters play critical roles in edge (growth front/reactive sites) growth as well as the nucleation process. Moreover, we find the agglomerated or linked cluster complexes become even more stable than individual clusters and will retard/prohibit the completion of growth for 2D full films. In this regard, reductive hydrogen atmosphere is helpful for full film growth as it can accelerate the rate control steps (selenization of cluster) and suppress the cluster agglomeration. In view of the stability and popularity of metal chalcogenide clusters (M_xC_{2x-n}, e.g., M_6C_8 and M_4C_6, M=Mo, W, Re, C=Se, Te)[27-29], our direct observations suggested the attachment, transport and agglomeration of intermediate chalcogenide clusters are essential steps in CVD synthesis of 2D TMDs.

RESULTS AND DISCUSSION

2D $ReSe_2$ morphology and characterizations. 2D $ReSe_2$ flakes (Figure 1a, also see Supporting Information (SI) Figure S1) in our experiments are grown on c-face sapphire by split-two-zone CVD (Figure 1b), using the ammonium perrhenate (NH_4ReO_4) and selenium (Se) as the source materials, and the synthesis temperature is 700 °C, refer to the Methods section for details. Observed in the optical micrographs (Figure 1c,d, SI Figure S2) and TEM images (Figure 1e), typical 2D $ReSe_2$ continuous flakes are synthesized, with thicknesses varying between 1-2 atomic layers (1L-2L). The obtained 2D $ReSe_2$ is largely polycrystalline, formed by nanometer-sized

grains. In Figure 1e, the crystal orientations (diamond Re chain, a direction) for each grain are highlighted by white arrows. Some nanometer-sized nuclei for 2D $ReSe_2$ as well as aggregates consisting of atomic-scale clusters (<1 nm) are dispersed on edges and the surfaces of 2D $ReSe_2$ (e.g., follow the red arrows in Figure 1e).

Differed from mechanically induced grain boundaries in 2D ReS_2[30], the polycrystalline 2D layer here with incommensurate grain boundaries is apparently formed by merging of randomly nucleated crystallites. The nuclei densities of the first and second layer are comparable (ca. 10^3 μm^{-2}). It is also noted the free edges of the $ReSe_2$ flakes prevalently follow the diamond chain *a* directions, irrespective of first or second atomic layers. The anisotropic nature of 2D $ReSe_2$ gives rise to the particular stripe-like morphologies of $ReSe_2$ crystals, following the principle a direction. More atomic force microscopy (AFM) and photoluminescence spectroscopy (PL) results on these 2D $ReSe_2$ flakes are presented in SI Figure S3-5. In general, the morphologies/thicknesses in our 2D $ReSe_2$ can be controlled by a few variables (temperature, growth duration, flow rates) in CVD process. In particular, we have found that with increased H_2 gas flow during CVD synthesis, the yielded surface roughness of 1L $ReSe_2$ significantly reduces (SI Figure S3). The enhanced uniformity in samples with increased H_2 also leads to higher strain levels retained in final 2D $ReSe_2$ samples (un-delamination of flakes), evidenced by the PL peak shift (SI Figure S5) and drops of polarized Raman intensities (SI Figure S6).

Identification of Re_xSe_y molecular clusters. According to the initial precursors in our experiment, vaporized Re_2O_7 and Se_n (n=3-8) molecules take the main portion in the atmosphere of CVD chamber (see Methods). However, except for the monoclinic 2D $ReSe_2$ film as expected in our growth product, the high resolution scanning TEM (STEM) (mainly through high angle annular dark field (HAADF) imaging) (Figure 2a-f) also reveals large quantity of Re_xSe_y clusters

attached to the surfaces/edges of as-grown 2D $ReSe_2$ flakes. The atomic structures and chemical compositions of such clusters are verified with multislice STEM image simulations (Figure 2e-f) and atomic-scale electron energy loss spectroscopy (EELS) results (Figure 2g and SI Figure S7). In most of the cases, these Re_xSe_y clusters are attached to the edges of monolayer or bilayer $ReSe_2$, while the atomic clusters residing away from edges can be attributed to the defective anchoring sites on van der Waals (vdW) surfaces of 2D $ReSe_2$ (Figure 1e, SI Figure S8 and SI Figure S9).

Key reactions and intermediate steps involved in growth. Rhenium oxide clusters can be safely excluded in our STEM images because they are highly water soluble[31] and cannot survive the wet transfer processes from growth substrates to TEM grids (see Methods). Our experiments, STEM image simulations and DFT atomistic simulations have captured the typical interfacial structures between Re_6Se_8 clusters and 2D $ReSe_2$ (Figure 2f and Figure 3a-h). Most of the survived clusters on edge or surfaces are covalently bonded through the linkage Se atoms. In agreement with the reported structures of the rhenium octahedron (Re_6) in Re_6Se_8 cluster complexes[32,33], we have experimentally confirmed the majority of clusters attached to our 2D samples contain six rhenium atoms. The projected STEM images for Re_6Se_8 clusters in different tilt angles with respect to the viewing direction (e- beam direction) are presented in Figure 2c-e. Due to the weaker contrast of Se atoms, the exact number of Se atoms in each cluster cannot be resolved by direct STEM imaging. Nevertheless, our DFT simulations have suggested that these octahedron clusters play crucial roles in reaction paths and have revealed further selenization processes of clusters toward 2D $ReSe_2$ (Figure 4). In addition, considering the prevalence of Se_8 molecules in CVD chamber, the Re_6Se_8 clusters are more likely to form compared to other clusters such as Re_2Se_4 or Re_4Se_6.

These *ex situ* observations do not preclude other possible reactants or intermediate species in high temperature CVD chambers. The weakly bonded clusters or atoms might have been

removed/escaped from $ReSe_2$ surfaces before observing them by STEM. However, with the high frequency of presence as observed in these post-CVD synthesis samples, it is reasonable to conclude that Re_6Se_8 clusters have high stability among all the reactants. Importantly, once the reactive sites (edges, defects on surfaces) are occupied by Re_6Se_8 clusters, further growth (selenization of Re_6Se_8) requests to overcome relative high energy barriers. In other words, CVD growth is significantly retarded by this intermediate stage, and the growth rate is mainly controlled by the conversion from Re_6Se_8 clusters to 2D $ReSe_2$. Hexarhenium cluster cores with the general formula $[Re_6Q_8]^{2+}$(Q = S, Se) own very high stability, which can serve as the building blocks in many kinds of ovel compound[28]. Thus, in our experiment we can directly observe such kind of cluster as the main reactant. While, the whole evolution process from the 3D face-capped octahedral core of Re_6Q_8 to 2D $ReSe_2$ formation is difficult to be determined via computational simulations by far. The Re/Se ratios in Re_6Q_8 and 2D $ReSe_2$ are 0.75 and 0.5, so additional four Se atoms (Re_6Se_{12}) should be added in the 2D $ReSe_2$ reactions. Here we used a simple DFT model to evaluate the chemical reaction under thermodynamic consideration by using Re_6Se_{12} as reactants. The adsorption energies of key intermediates are studied and depicted in Figure 4.

Our DFT simulations have given the key reaction paths and revealed that the further selenization process of these clusters should proceed with high edge selectivity along edges along a direction. The corresponding absorption energies of Re_6Se_{12} (4 Se atoms are subsequently added onto Re_6Se_8 cluster) and the whole reaction energies are much lower than the case along *b* edges by energy gaps of -1.90 and -1.89 eV under thermodynamic consideration (Figure 4). The result is in agreement with the preferred edges for 2D clusters formation in our STEM observations (Figure 3a-d). It also well explains why the 2D $ReSe_2$ tends to grow along the diamond Re chain *a* direction and form elongated rectangles in morphology. Besides, each diamond cell in 2D $ReSe_2$ contains

four rhenium atoms, mismatched with the six atoms in each cluster. Hence the completion of selenization (from Re_6Se_8 cluster to 2D $ReSe_2$ layer) should sometimes leave bi-Re atom structures on edges (Figure 3g captures intermediate structures). These locations will be easier to trap another Re_6Se_8 cluster, as observed in Figure 3g. For the same reason, Re_6Se_8 clusters prefer to aggregate in odd numbers on growth edges, even number Re_6Se_8 clusters are much easier to form 2D $ReSe_2$.

Re_6Se_8 clusters favor the further aggregation as cluster agglomerates sized from 1 nm to few nanometer (Figure 2a,b, Figure 5a and SI Figure S9). The clusters form one-dimensional chain-like structures (Figure 5a). These cluster complexes are highly stable and embedded in the 1L or 2L $ReSe_2$. Experimentally, the density of such cluster complexes as well as survival individual clusters can be reduced by higher concentration of hydrogen in CVD atmosphere (SI Figure S8), implying hydrogen is the key for reducing cluster aggregation and triggering conversion from clusters into 2D structure. The cluster agglomerates embedded in the 2D layers can introduce large defects (holes) in 2D films after removal/evaporation of clusters, therefore maintaining a reductive hydrogen environment in CVD growth is indispensable for 2D full film growth.

Re_6Se_8 cluster is highly stable, Figure 5b shows a single cluster can withstand high energy e- beam irradiation, while only cluster rotation is found. During CVD growth, these clusters can be freely transported in CVD atmosphere or on the solid (substrate/product) surfaces. Our STEM results directly unraveled the nucleation process. The observed smallest nuclei for 2D $ReSe_2$ (on $ReSe_2$ substrate) is smaller than 1 nm (Figure 3b), (ca. two by two unit cells of monoclinic $ReSe_2$). Regarding the nucleation probability, as we can observe in 2D samples, a lot of nuclei are stable even in single Re_6Se_8 cluster form or bi-cluster form (Figure 1e). With the undergoing reactions, these covalently surface-trapped clusters on surfaces of 2D $ReSe_2$ can easily develop into larger islands of $ReSe_2$ epi-layers (Figure 3e-h). In contrast, the kinetics of individual metal or

chalcogenide atoms (in some previous growth models[2]) are much faster. Therefore the nucleation rate of 2D $ReSe_2$ is greatly enhanced by such Re_6Se_8 clusters, and the kinetical (non-thermal) growth is also greatly strengthened due to the existence of such molecular clusters. To suppress unwanted nucleation and epi-layer growth, and to achieve the ideal Frank-van der Merwe (FM) layer-by-layer growth, high quality layers with minimum atomic defects and vacancies (anchoring sites for clusters) is favored.

Our observations do not rule out other growth mechanisms, such as direct individual atomic growth or selenization from oxides. Nonetheless, evidenced by our direct STEM observations, Re_6Se_8 clusters can easily and stably bond to edges as well as surfaces of 2D $ReSe_2$, giving rise to higher reaction possibilities and yielding the 2D structures. The preferential adsorption of Re_6Se_8 clusters on different edges and the retarded transport of Re_6Se_8 clusters along edges/on surfaces significantly alter the growth kinetics and the final product morphologies. Some unexpected effects might even occur, for instance, due to the preferred bonding of Re_6Se_8 clusters with atomic vacancies and the enhanced Se vacancies at higher temperatures, the nucleation rate for epi-layers actually increases with temperature, violating normal principles for 2D material growth whereas higher temperature yields higher uniformity[34].

CONCLUSION

Our atomic-scale observations combined with theoretical simulations on the intermediate stages of the 2D $ReSe_2$ growth directly reveal the reaction paths in CVD process, with implications for general 2D TMD materials growth. Based on our observations, here we propose a simple model for APCVD of 2D TMDs. It consists of two-step reactions: (1) Reduction reactions with chalcogenides and hydrogen in atmosphere to form M_xC_{2x-n} clusters (M=transition metal,

C=chalcogenide)). (2) Attachment of M_xC_{2x-n} clusters to the growth fronts and conversion into 2D TMD layers with the aid of hydrogen. The unveiled reaction paths are of great significance to understand the nucleation and growth kinetics of 2D TMD materials, and will benefit the growth control on thickness and morphology for such emergent group of materials.

EXPERIMENTAL SECTION

Materials

All chemicals were utilized as received without further processing. Ammonium perrhenate (NH_4ReO_4, Sigma-Aldrich, ⩾ 99.999%), selenium (Sigma-Aldrich, ⩾ 99.99%) were acting as precursors and c-face sapphires were used as substrate. A4 liquid Poly (methyl methacrylate) (PMMA) was employed as transfer medium and Potassium hydroxide solution (KOH, Honeywell, ⩾ 85%) was used for detaching. Acetone (AQA, ⩾ 99.5%) was used for PMMA removal after transfer. The ultrapure water was produced by Milli-Q water-purification system.

Chemical vapor deposition (CVD) growth of rhenium diselenide ($ReSe_2$)

The $ReSe_2$ flakes were grown on c-face sapphire in atmospheric CVD system with double heating zones. Initially, 1.5 mg NH_4ReO_4 was sprayed in the quartz boat in the center of downstream zone and 10.0 mg selenium source was placed in another quartz boat in the center of upstream zone. 1 cm × 1 cm c-face sapphire was facing downward towards crushed molecular sieves which were placed above the Re source. 300 sccm argon gas was pumped in the quartz tube for 10 minutes prior to the beginning of the heating program. Then the upstream zone was heated up to 400 °C at 20 °C min^{-1} and held for 10 minutes. Simultaneously, the downstream zone was heated at 34 °C

min^{-1} up to 700 °C and held for 10 minutes. During the growth, argon gas flow was adjusted to 80 sccm and hydrogen gas flow was set at 1-5 sccm. Selenium vapor was carried by Argon and hydrogen gas onto the c-face sapphire substrate. Both zones cooled down naturally right at the completion of the heating program.

$ReSe_2$ transfer

The c-face sapphire substrate with as-grown $ReSe_2$ was firstly spin-coated with 1-2 drops of PMMA and at 800 r.p.m. min^{-1} for 10 seconds followed by 3000 r.p.m. min^{-1} for 1 minute. Then the as-formed PMMA/$ReSe_2$ film was detached from the c-face sapphire substrate by floating on 75 °C 1 mol L^{-1} KOH for 20-30 minutes. Subsequently, the PMMA/$ReSe_2$ film floated on ultrapure water for washing purpose for 3 times, each time at 10 minutes. Next, the PMMA/$ReSe_2$ film was covered onto a QuantifoilTM TEM grid and after 2-hour natural drying the PMMA was carefully etched away by acetone vapor.

Topographic measurement

The as-grown $ReSe_2$ on c-face sapphire substrate was firstly observed under optical microscopy (ZEISS Imager.A2m) under bright field, dark field and polarization light of 70 ° and 110 °, which illustrated the $ReSe_2$ flakes distribution and the inner subdomains of each flake. Then atomic force microscopy (HITACHI, AFM5300E) was applied to check the morphologic information of $ReSe_2$, employing SI-DF40P2 silicon tip (Hitachi).

Optical and structural properties characterization

Photoluminescence spectra (Renishaw, inVia confocal) was employed to detect the optical properties of as-grown $ReSe_2$. The laser wavelength is 633 nm, with grating of 1800 g/mm. The signals were collected under 50 × lens (0.75 N.A.) and the laser spatial resolution is around 1 μm. The laser power is 0.6 mV and for each single spectrum measurement, the exposure time is 10 seconds.

Angle-resolved Raman spectroscopy

The angle-resolved Raman measurement was conducted at the excitation laser length of 785 nm with grating of 1200 g/mm, under 50 × lens (0.75 N.A.). The polarized Raman setup includes a motorized half-wave plate, a half-wave plate and a linear polarizer. The Raman signals were collected at 0 ° and 70 ° rotation of incident polarized light. Scattered light goes to the CCD through the half-wave plate and linear polarizer.

Transmission electron microscopy (TEM), scanning transmission electron microscopy (STEM) high angle annular dark field (HAADF) and electron energy loss spectroscopy (EELS)

The high-resolution TEM and STEM morphologic images, high resolution STEM HAADF images and EELS were obtained by JEM-ARM200F TEM instrument equipped with a CEOS spherical (Cs) aberration (probe) corrector working under 60 kV. The beam current is 0.3 pA nm^{-1} and the beam probe size is 1.5 angstrom. Average background subtracting filtering (ABSF) is applied to reduce the noise of STEM-HAADF images. The EELS acquisition is completed with the Gatan Quantum^{TM}, beam probe size ca. 1.5 angstrom, convergence angle 29 mrad, collection angle 35

mrad and exposure time 2 s are applied. The STEM HAADF image simulations are completed using QSTEM software with the same set of conditions as STEM experiments. The defocus and the spherical aberration are set as Scherzer focus and 1 μm, respectively. The other settings remain default.

DFT simulation

Spin-polarized density function theory (DFT) calculations are performed by using the Vienna *ab initio* Simulation Package (VASP) program package[35,36] within the projector augmented wave (PAW)[37] to explore geometries and electronic properties of ReS_2. The exchange-correlation interactions are described with the generalized gradient approximation (GGA)[38] in the form of the Perdew, Burke, and Ernzernhof (PBE) functional[39]. The kinetic energy cutoff for the plane-wave basis set is chosen as 450 eV, and the distance of vacuum layer is set to be more than 20 Å, which is sufficient large to avoid interlayer interactions. The DFT-D3 scheme of Grimme for the vdW correction[40] is applied on 2D-$ReSe_2$. The pristine slab contains 96 Re and 216 Se atoms. The electronic SCF tolerance is set to 10^{-5} eV. Fully relaxed geometries and lattice constant are obtained by optimizing all atomic positions until the Hellmann–Feynman forces are less than 0.03 eV/Å with the gamma point sampling.

Figures and Figure Captions

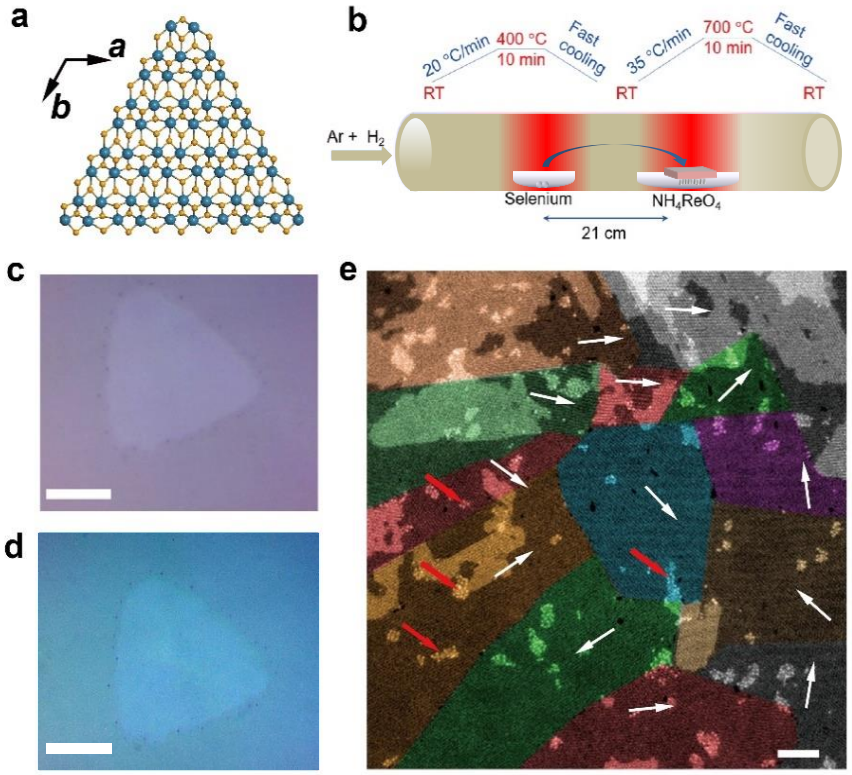

Figure 1. CVD Synthesis of 2D $ReSe_2$. (a) Atomic models for 2D $ReSe_2$, *a* and *b* crystal directions are highlighted, *a* is along Re diamond chain direction. Re atom (blue), Se atom (yellow). (b) Scheme of split-zone CVD growth. (c),(d) Optical images (non-polarized and polarized) for as grown monolayer 2D $ReSe_2$ flake, showing anisotropic stripe patterns. Scale bars = 10 µm. (e) TEM HAADF image for as grown 2D $ReSe_2$. Different grains are false colored for contrast enhancement. Red arrows mark the cluster aggregates. White arrows mark the *a* direction for each grain. Scale bar = 10 nm.

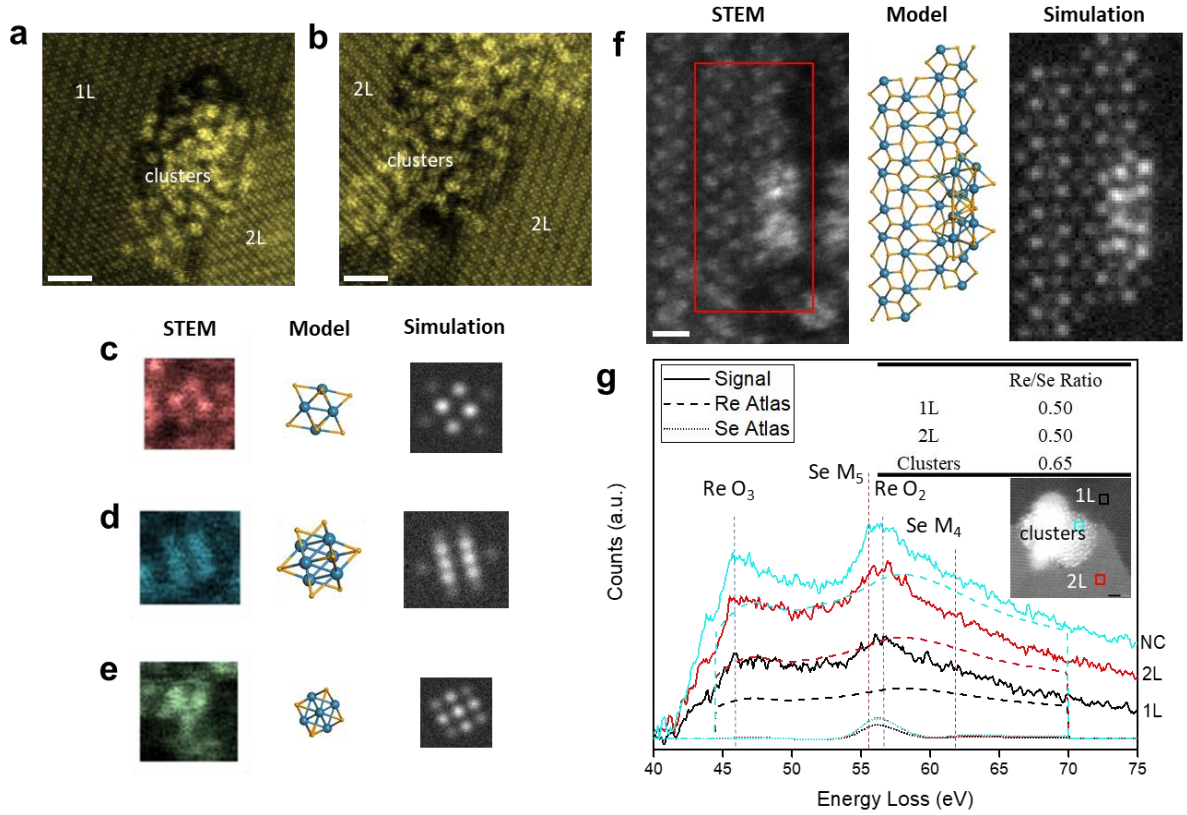

Figure 2. STEM characterizations of Re_6Se_8 clusters. (a),(b) Re_6Se_8 cluster aggregates residing in holes of mono- and bi-layer $ReSe_2$. Scale bars = 2 nm. (c)-(e) STEM-HAADF images, DFT derived atomic models and STEM image simulations of Re_6Se_8 clusters in different orientations. (f) STEM image, DFT derived atomic model and STEM image simulations for two Re_6Se_8 clusters attached to the edge of 2D $ReSe_2$. Scale bar = 0.5 nm. (g) EELS results (background subtracted) for Re_6Se_8 cluster aggregates, EELS quantification consistently gives higher Re/Se ratio in clusters than in 2D $ReSe_2$ layers.

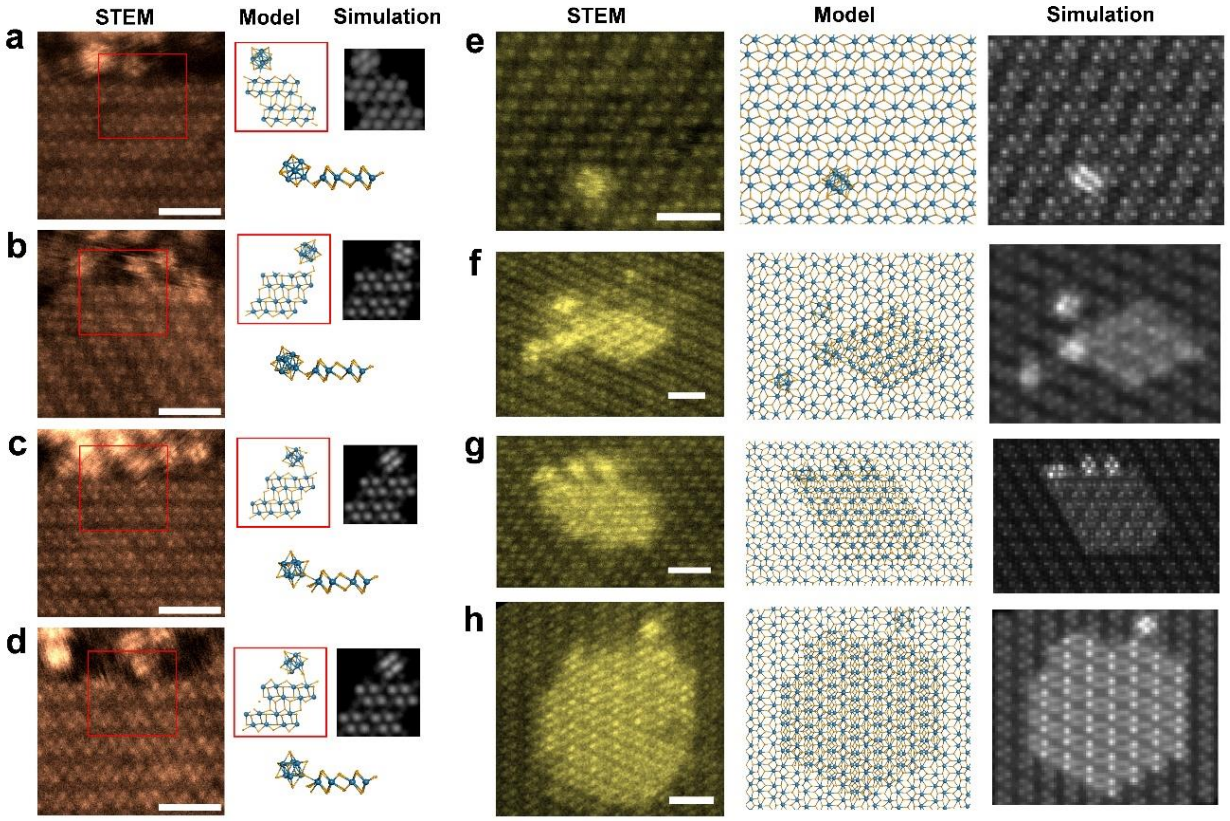

Figure 3. Re_6Se_8 clusters and nucleation. (a)-(d) STEM image, DFT derived atomic model and STEM image simulation for Re_6Se_8 clusters anchored on different edges of 2D $ReSe_2$ through Se linkage atoms. Scale bars =1 nm. (e)-(h) STEM image, atomic model and STEM image simulation for Re_6Se_8 clusters anchored on monolayer $ReSe_2$ surfaces and crystal nuclei for epi-layers of 2D $ReSe_2$ with Re_6Se_8 clusters attached on edges. Scale bars = 1 nm.

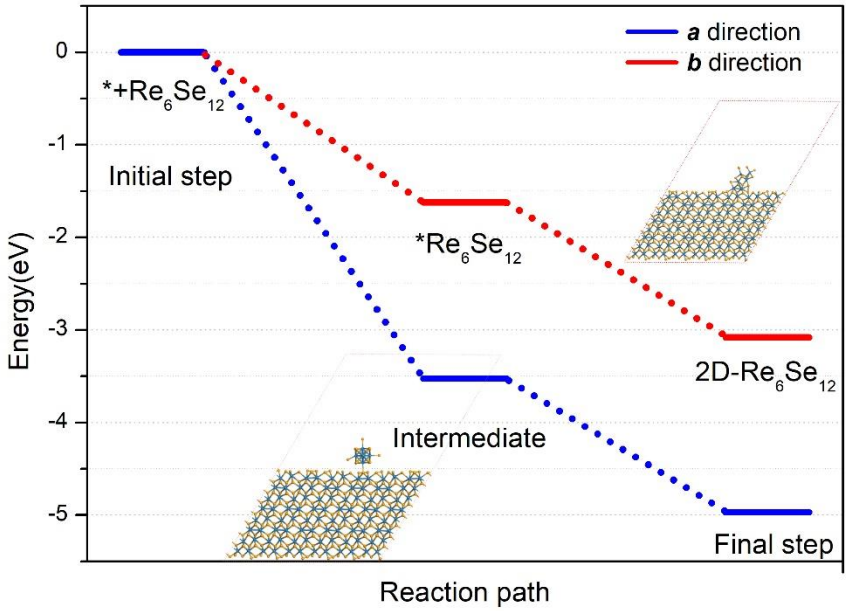

Figure 4. Reaction energy profile for selenization process along edges of *a* (blue) and *b* (red) by DFT calculations. Initial and final steps involve gas phase Re_6Se_{12} cluster adsorbed on different edges to 2D cluster formation.

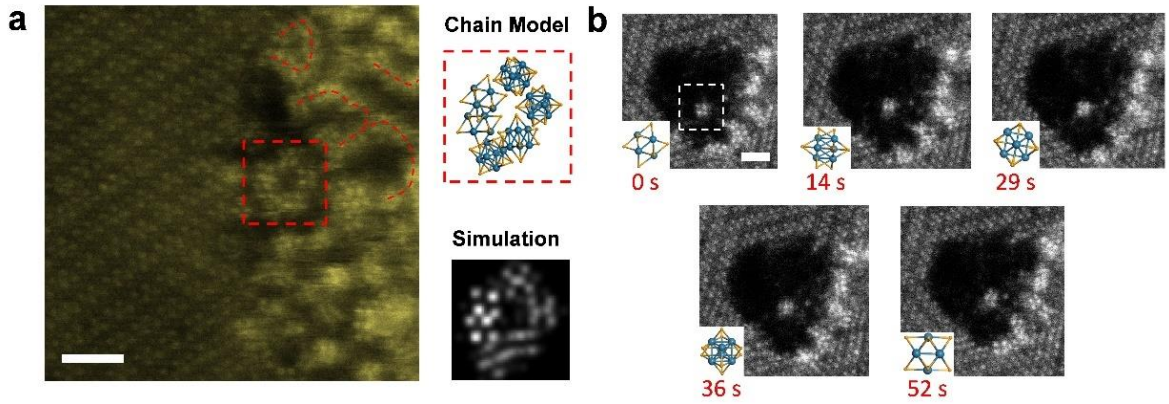

Figure 5. Stable Re_6Se_8 clusters and aggregates. (a) STEM image, atomic model and image simulation for cluster aggregates. Chain-like structures are highlighted by red dashed lines and boxes in STEM images. Scale bar = 1 nm. (b) Stability of single Re_6Se_8 cluster under e beam irradiation for 52 s. Rotation of cluster (center in white dashed box) is noted, corresponding atomic models for Re_6Se_8 cluster of each time are embedded in lower left corners. Scale bar = 1 nm.

ASSOCIATED CONTENT

The Supporting Information is available free of charge at XXXXXX.

AUTHOR INFORMATION

Corresponding Authors

Thuc Hue Ly - Department of Chemistry and Center of Super-Diamond & Advanced Films (COSDAF), City University of Hong Kong, Kowloon, Hong Kong 999077, China & City University of Hong Kong Shenzhen Research Institute, Shenzhen 518057, China; Email: thuchly@cityu.edu.hk

Jiong Zhao - Department of Applied Physics, The Hong Kong Polytechnic University, Kowloon, Hong Kong 999077, China & Polytechnic University of Hong Kong Shenzhen Research Institute, Shenzhen 518057, China; Email: jiongzhao@polyu.edu.hk

Qingming Deng - Physics department and Jiangsu Key Laboratory for Chemistry of Low-Dimensional Materials, Huaiyin Normal University, Huaian 223300, China; Email: qingmingdeng@gmail.com

Authors

Xin Chen - Department of Chemistry and Center of Super-Diamond & Advanced Films (COSDAF), City University of Hong Kong, Kowloon, Hong Kong 999077, China & City University of Hong Kong Shenzhen Research Institute, Shenzhen 518057, China

Lok-Wing Wong - Department of Applied Physics, The Hong Kong Polytechnic University, Kowloon, Hong Kong 999077, China & Polytechnic University of Hong Kong Shenzhen Research Institute, Shenzhen 518057, China

Lingli Huang - Department of Chemistry and Center of Super-Diamond & Advanced Films (COSDAF), City University of Hong Kong, Kowloon, Hong Kong 999077, China & City University of Hong Kong Shenzhen Research Institute, Shenzhen 518057, China

Fangyuan Zheng - Department of Applied Physics, The Hong Kong Polytechnic University, Kowloon, Hong Kong 999077, China & Polytechnic University of Hong Kong Shenzhen Research Institute, Shenzhen 518057, China

Rui Huang - Physics department and Jiangsu Key Laboratory for Chemistry of Low-Dimensional Materials, Huaiyin Normal University, Huaian 223300, China

Shu Ping Lau - Department of Applied Physics, The Hong Kong Polytechnic University, Kowloon, Hong Kong 999077, China & Polytechnic University of Hong Kong Shenzhen Research Institute, Shenzhen 518057, China

Chun-Sing Lee - Department of Chemistry and Center of Super-Diamond & Advanced Films (COSDAF), City University of Hong Kong, Kowloon, Hong Kong 999077, China & City University of Hong Kong Shenzhen Research Institute, Shenzhen 518057, China

Author Contributions

T.H.L conceived the project and supervised the research. X.C, L.H, C.S.L and T.H.L performed the sample synthesis and characterizations excluding TEM/STEM. L.W.W, F.Z, S.P.L and J.Z performed TEM/STEM experiments and analysis. R.H and Q.D performed DFT calculations and analysis. T.H.L, J.Z, Q.D, X.C and L.W.W co-wrote the manuscript. All authors read and approved the final manuscript.

ACKNOWLEDGMENT

This work was supported by the National Science Foundation of China (Project No. 51872248, 21703076, 51922113), the Hong Kong Research Grant Council under the Early Career Scheme (Project No. 25301018), the Hong Kong Research Grant Council General Research Fund (Project No. 11300820, 15302419), City University of Hong Kong (Project No. 9680241, 9229074), The Hong Kong Polytechnic University (Project No. 1-ZVGH and ZVRP), Shenzhen Science, Technology and Innovation Commission (Project No. JCYJ20200109110213442). Natural Science Foundation of Jiangsu Province of China (Project No. BKBK202100XX), and Natural Science Foundation of the Jiangsu Higher Education Institutions of China (No.18KJA140001).

REFERENCES

1. Liu, E.; Fu, Y.; Wang, Y.; Feng, Y.; Liu, H.; Wan, X.; Zhou, W.; Wang, B.; Shao, L.; Ho, C.-H.; Huang, Y.-S.; Cao, Z.; Wang, L.; Li, A.; Zeng, J.; Song, F.; Wang, X.; Shi, Y.; Yuan, H.; Hwang, H. Y.; Cui, Y.; Miao, F.; Xing, D. Integrated Digital Inverters Based on Two-Dimensional Anisotropic ReS_2 Field-Effect Transistors. *Nat. Commun.* **2015**, 6, 6991-6997.

2. Li, J.; Zhou, Q.; Yuan, C.; Cheng, P.; Hu, X.; Huang, W.; Gao, X.; Wang, X.; Jin, M.; Nötzel, R., Direct growth of vertically aligned ReSe2 nanosheets on conductive electrode for electro-catalytic hydrogen production. *J. Colloid Interf. Sci.* **2019**, 553, 699-704.

3. Xing, L.; Yan, X.; Zheng, J.; Xu, G.; Lu, Z.; Liu, L.; Wang, J.; Wang, P.; Pan, X.; Jiao, L., Highly crystalline ReSe2 atomic layers synthesized by chemical vapor transport. *InfoMat* **2019**, 1, 552-558.

4. Cui, F.; Li, X.; Feng, Q.; Yin, J.; Zhou, L.; Liu, D.; Liu, K.; He, X.; Liang, X.; Liu, S., Epitaxial growth of large-area and highly crystalline anisotropic ReSe2 atomic layer. *Nano Res.* **2017**, 10, 2732-2742.

5. Shi, Y.; Li, H.; Li, L. J. Recent Advances in Controlled Synthesis of Two-Dimensional Transition Metal Dichalcogenides via Vapour Deposition Techniques. *Chem. Soc. Rev.* **2015**, 44, 2744-2756.

6. Jiang, S.; Yang, J.; Shi, Y.; Zhao, J.; Xie, C.; Zhao, L.; Fu, J.; Yang, P.; Huan, Y.; Xie, Q.; Jiang, H.; Zhang, Q.; Wang, X.; Su, F.; Zhang, Y. Salt-assisted growth and ultrafast photocarrier dynamics of large-sized monolayer $ReSe_2$. *Nano Res.* **2020**, 13, 667–675.

7. Shi, J.; Ma, D.; Han, G.-F.; Zhang, Y.; Ji, Q.; Gao, T.; Sun, J.; Song, X.; Li, C.; Zhang, Y.; Lang, X.-Y.; Zhang, Y.; Liu, Z. Controllable Growth and Transfer of Monolayer MoS_2 on Au Foils and Its Potential Application in Hydrogen Evolution Reaction. *ACS Nano* **2014**, 8, 10196-10204.

8. Etzkorn, J.; Therese, H. A.; Rocker, F.; Zink, N.; Kolb, U.; Tremel, W. Metal-Organic Chemical Vapor Depostion Synthesis of Hollow Inorganic-Fullerene-Type MoS_2 and $MoSe_2$ Nanoparticles. *Adv. Mater.* **2005**, 17, 2372-2375.

9. Xie, C.; Jiang, S.; Zou X.; Sun, Y.; Zhao, L.; Hong, M.; Chen, S.; Huan, Y.; Shi J.; Zhou, X.; Zhang, Z.; Yang, P.; Shi, Y.; Liu, P.; Zhang, Q.; Gao, P.; Zhang, Y. Space-confined growth of monolayer ReSe2 under a graphene layer on Au foils. *Nano Res.* **2019**, 12, 149–157.

10. Chareev, D. A.; Evstigneeva, P.; Phuyal, D.; Man, G. J.; Rensmo, H.; Vasiliev, A. N.; Abdel-Hafiez, M., Growth of transition-metal dichalcogenides by solvent evaporation technique. *Crys. Growth Des.* **2020**, 20, 6930-6938.

11. Zhang, Y.; Yao, Y.; Sendeku, M. G.; Yin, L.; Zhan, X.; Wang, F.; Wang, Z.; He, J. Recent Progress in CVD Growth of 2D Transition Metal Dichalcogenides and Related Heterostructures. *Adv. Mater.* **2019**, 31, e1901694.

12. Xue, H.; Wu, G.; Zhao, B.; Wang, D.; Wu, X.; Hu, Z. High-Temperature In Situ Investigation of Chemical Vapor Deposition to Reveal Growth Mechanisms of Monolayer Molybdenum Disulfide. *ACS Appl. Electro.Mater.* **2020**, 2, 1925-1933.

13. Huang, L.; Yang, T.; Wong, L. W.; Zheng, F.; Chen, X.; Lai, K. H.; Liu, H.; Thi, Q. H.; Shen, D.; Lee, C. S., Redox Photochemistry on Van Der Waals Surfaces for Reversible Doping in 2D Materials. *Adv. Func. Mater.* **2021**, 31, 2009166.

14. Huang, L.; Thi, Q. H.; Zheng, F.; Chen, X.; Chu, Y. W.; Lee, C.-S.; Zhao, J.; Ly, T. H., Catalyzed kinetic growth in two-dimensional MoS_2. *J. Am. Chem. Soc.* 2020, 142, 13130-13135.

15. An, G. H.; Yun, S. J.; Lee, Y. H.; Lee, H. S. Growth Mechanism of Alternating Defect Domains in Hexagonal WS_2 via Inhomogeneous W-Precursor Accumulation. *Small* **2020**, 16, 2003326.

16. Hong, S.; Krishnamoorthy, A.; Rajak, P.; Tiwari, S.; Misawa, M.; Shimojo, F.; Kalia, R. K.; Nakano, A.; Vashishta, P. Computational Synthesis of MoS_2 Layers by Reactive Molecular Dynamics Simulations: Initial Sulfidation of MoO_3 Surfaces. *Nano Lett.* **2017**, 17, 4866-4872.

17. Zhu, D.; Shu, H.; Jiang, F.; Lv, D.; Asokan, V.; Omar, O.; Yuan, J.; Zhang, Z.; Jin, C. Capture the Growth Kinetics of CVD Growth of Two-Dimensional MoS_2. *npj 2D Mater. and Appl.* **2017**, 1, 8.

18. Ji, Q.; Zhang, Y.; Zhang, Y.; Liu, Z. Chemical Vapour Deposition of Group-VIB Metal Dichalcogenide Monolayers: Engineered Substrates from Amorphous to Single Crystalline. *Chem. Soc. Rev.* **2015**, 44, 2587-2602.

19. Shao, P.; Ding, L.-P.; Ding, F. Mechanism of MoS_2 Growth on a Au(111) Surface: An Ab Initio Molecular Dynamics Study. *Chem. Mater.* **2021**, 33, 3241-3248.

20. Kim, S. Y.; Kwak, J.; Ciobanu, C. V.; Kwon, S. Y. Recent Developments in Controlled Vapor-Phase Growth of 2D Group 6 Transition Metal Dichalcogenides. *Adv. Mater.* **2019**, 31, e1804939.

21. Barja, S.; Refaely-Abramson, S.; Schuler, B.; Qiu, D. Y.; Pulkin, A.; Wickenburg, S.; Ryu, H.; Ugeda, M. M.; Kastl, C.; Chen, C.; Hwang, C.; Schwartzberg, A.; Aloni, S.; Mo, S. K.; Ogletree, D. F.; Crommie, M. F.; Yazyev, O. V.; Louie, S. G.; Neaton, J. B.; Weber-Bargioni, A. Identifying

Substitutional Oxygen as A Prolific Point Defect in Monolayer Transition Metal Dichalcogenides. *Nat. Commun.* **2019**, 10, 3382-3390.

22. Fan, X. G.; Wagner, S.; Schadlich, P.; Speck, F.; Kataria, S.; Haraldsson, T.; Seyller, T.; Lemme, M. C.; Niklaus, F. Direct Observation of Grain Boundaries in Graphene through Vapor Hydrofluoric Acid (VHF) Exposure. Sci. Adv. **2018**, 4, 5170-5179.

23. Kim, H.; Han, G. H.; Yun, S. J.; Zhao, J.; Keum, D. H.; Jeong, H. Y.; Ly, T. H.; Jin, Y.; Park, J. H.; Moon, B. H.; Kim, S. W.; Lee, Y. H. Role of Alkali Metal Promoter in Enhancing Lateral Growth of Monolayer Transition Metal Dichalcogenides. *Nanotechnology* **2017**, 28, 36LT01.

24. Liu, K. K.; Zhang, W. J.; Lee, Y. H.; Lin, Y. C.; Chang, M. T.; Su, C.; Chang, C. S.; Li, H.; Shi, Y. M.; Zhang, H.; Lai, C. S.; Li, L. J. Growth of Large-Area and Highly Crystalline MoS_2 Thin Layers on Insulating Substrates. *Nano Lett.* **2012**, 12, 1538-1544.

25. Yue, R.; Nie, Y.; Walsh, L. A.; Addou, R.; Liang, C.; Lu, N.; Barton, A. T.; Zhu, H.; Che, Z.; Barrera, D. Nucleation and Growth of WSe_2: Enabling Large Grain Transition Metal Dichalcogenides. *2d Mater.* **2017**, 4, 045019.

26. Cain, J. D.; Shi, F.; Wu, J.; Dravid, V. P. Growth Mechanism of Transition Metal Dichalcogenide Mon-olayers: the Role of Self-Seeding Fullerene Nuclei. *ACS Nano* **2016**, 10, 5440-5445.

27. Murugan, P.; Kumar, V.; Kawazoe, Y.; Ota, N. Atomic Structures and Magnetism in Small MoS2 and WS2 Clusters. *Phys. Rev. A* **2005**, 71, 063203.

28. Zheng, Z.; Long, J. R.; Holm, R. H. A Basis Set of Re_6Se_8 Cluster Building Blocks and Demonstration of Their Linking Capability: Directed Synthesis of an $Re_{12}Se_{16}$ Dicluster. *J. Am. Chem. Soc.* **1997**, 119, 2163-2171.

29. Gray, T. G.; Rudzinski, C. M.; Nocera, D. G.; Holm, R. H. Highly Emissive Hexanuclear Rhenium(III) Clusters Containing the Cubic Cores $[Re_6S_8]^{2+}$ and $[Re_6Se_8]^{2+.}$ *Inorg. Chem.* **1999**, 38, 5932-5933.

30. Zheng, F.; Huang, L.; Wong, L. W.; Han, J.; Cai, Y.; Wang, N.; Deng, Q.; Ly, T. H.; Zhao, J. The Mobile and Pinned Grain Boundaries in 2D Monoclinic Rhenium Disulfide. *Adv. Sci.* **2020**, 7, 2001742.

31. Kuhn, F. E.; Herrmann, W. A. Rhenium-Oxo and Rhenium-Peroxo Complexes in Catalytic Oxidations. *Struct. Bond.* **2000**, 97, 213-236.

32. Zheng, Z., Selby, H. & Roland, B. The First `Hexa-Aqua-' Complex of the $[Re_6Se_8]^{2+}$ Cluster Core, $[Re_6Se_8(OH)_2(H_2O)_4]$. *Acta Crystallogr. E* **2001**, 57, i77-i79.

33. Gabriel, J. C. P.; Boubekeur, K.; Uriel, S.; Batail, P. Chemistry of hexanuclear rhenium chalcohalide clusters. *Chemical Reviews,* **2001**, 101, 2037-2066.

34. Li, X.; Cui, F.; Feng, Q.; Wang, G.; Xu, X.; Wu, J.; Mao, N.; Liang, X.; Zhang, Z.; Zhang, J.; Xu, H. Controlled Growth of Large-Area Anisotropic ReS_2 Atomic Layer and Its Photodetector Application. *Nanoscale* **2016**, 8, 18956-18962.

35. Kresse, G.; Furthmüller, J. Efficient Iterative Schemes for Ab Initio Total-Energy Calculations Using A Plane-Wave Basis Set. *Phys. Rev. B* **1996**, 54, 11169-11186.

36. Kresse, G.; Furthmüller, J., Efficiency of Ab-Initio Total Energy Calculations for Metals and Semiconductors Using A Plane-Wave Basis Set. Com. *Mater. Sci.* **1996**, 6, 15-50.

37. Blöchl, P. E. Projector Augmented-Wave Method. *Phys rev. B* **1994**, 50, 17953-17979.

38. Perdew, J. P.; Burke, K.; Ernzerhof, M. Generalized Gradient Approximation Made Simple. *Phys Rev. Lett.* **1996**, 77, 3865-3868.

39. Perdew, J. P.; Ernzerhof, M.; Burke, K. Rationale for Mixing Exact Exchange with Density Functional Approximations. *J. Chem. Phys.* **1996**, 105, 9982-9985.

40. Grimme, S.; Antony, J.; Ehrlich, S.; Krieg, H. A Consistent and Accurate Ab Initio Parametrization of Density Functional Dispersion Correction (DFT-D) for the 94 Ele-ments H-Pu. *J. Chem. Phys.* **2010**, 132, 154104.

TOC Graphic: